

On flame-flow interaction in forward smoldering

Irina Brailovsky* Peter Gordon † Gregory Sivashinsky‡

February 6, 2008

Abstract

Departing from the classical Burke-Schumann theory for diffusion flames, a reduced model for the description of the evolving wave front in forward smoldering is derived. The model is then used to describe the fingering instability induced by the increase in porosity, which results from the solid fuel depletion. The cusp-leading nature of the fingering pattern is revealed, which is opposite to the cusp-trailing structure typical of premixed gas cellular/wrinkled flames.

1 Introduction

One of the most effective strategies in analyzing combustion waves (both self-sustained and driven) is the reduction of the associated dynamical system to a geometrical problem dealing directly with the evolving interface representing location of the reaction zone (wave front). Reduced models are highly informative for elucidation of the physical mechanisms involved. Moreover, since the reduced model generally has a lower dimensionality than the original system, it is also often advantageous for numerical simulations. The objective of the present study is the formulation of a reduced model for flame-flow interaction in forward smoldering which attracts much attention due to its relevance to fire safety, as well as several technological processes such as high-temperature synthesis and combustion-assisted fossil fuel recovery. Although the forward smoldering has been extensively explored both experimentally and theoretically [1-12], its hydrodynamic aspects have received relatively little attention. A notable exception is the work of Aldushin and Matkowsky [10] where a comprehensive stability analysis was undertaken including calculation of the solitary finger sustained by the porosity increase due to depletion of the solid reactant.

2 Formulation

Forward smoldering is a heterogeneous combustion where an oxidizing gas is forced into a porous solid fuel through the solid reaction products. The burning zone is propagated in a direction concurrent with the oxidant stream. The forward smoldering may therefore be perceived as a diffusion flame driven by the underlying flow-field (Figure 1). In the present study the discussion is restricted to the fast-chemistry limit (large Damköhler number) where there is a negligible leakage of reactants across the reaction zone (Burke-Schumann). This limit is of great practical interest since away from the extinction point Damköhler numbers are indeed generally large. The problem of forward

*Department of Mathematical Sciences, Tel Aviv University, Tel Aviv 69978, Israel; brailir@post.tau.ac.il

†Department of Mathematical Sciences, New Jersey Institute of Technology, Newark, NJ 07102 USA; peterg@njit.edu

‡Department of Mathematical Sciences, Tel Aviv University, Tel Aviv 69978, Israel; grishas@post.tau.ac.il, corresponding author

smoldering thus reduces to a Stefan-like free-boundary problem for the oxygen mass-fraction. It involves minimum physical ingredients and displays the salient features of smolder-flow interaction in their most simple and transparent form. In the constant-density approximation, adopted in this study, the pertinent diffusion-advection equation reads,

$$\rho_g(a_t + \mathbf{u} \cdot \nabla a) = \rho_g D \nabla^2 a, \quad (1)$$

where

$$\nabla \cdot \mathbf{u} = 0. \quad (2)$$

Here a is the mass-fraction of oxygen, entirely consumed within the reaction zone. Hence, $a = 0$ ahead of the advancing interface; $a = a_0$ far behind the interface. The rate of oxygen consumption is specified by the jump condition,

$$\rho_g D [\nabla a \cdot \mathbf{N}]|_{\text{interface}} = \rho_s b_0 V_n. \quad (3)$$

Here D is the molecular diffusivity assumed constant, b_0 is the mass-fraction of solid fuel, also entirely consumed within the reaction zone. \mathbf{u} is the gas flow velocity, \mathbf{N} is a unit normal to the interface directed towards the fluid ahead of the interface. ρ_g, ρ_s are the effective densities of gaseous and solid reactants, respectively ($\rho_s \gg \rho_g$). V_n is the normal velocity of the interface, whose evaluation in terms of the underlying flow-field \mathbf{u} and parameters of the system, is the principal objective of the current study.

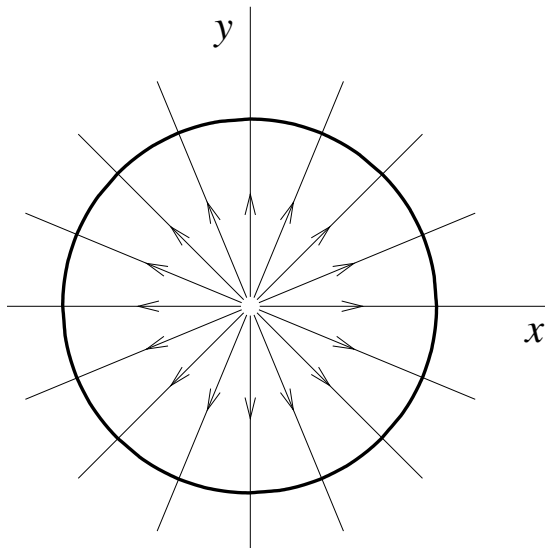


Figure 1: Diagram illustrating outward spreading circular diffusion flame driven by a radial flow of oxidant. Arrows indicate direction of streamlines. Bold line corresponds to the flame front.

Eqs. (1) (2) are augmented by the momentum (Darcy) equation,

$$\nabla P = -\frac{1}{\lambda} \mathbf{u}, \quad (4)$$

where P is the pressure, and λ is the mobility of the system, affected by the smoldering.

For simplicity of further analysis, yet without much detriment to general understanding, the current discussion is restricted to the stepwise dependency (see also Sec. 8),

$$\begin{aligned} \lambda &= \lambda_a \quad \text{at} \quad a = 0, \\ \lambda &= \lambda_b \quad \text{at} \quad 0 < a \leq 1. \end{aligned} \tag{5}$$

The subscripts a and b mean *ahead* and *behind* the smolder front.

3 Intrinsic geometry and front-attached coordinates

In order to make the analysis tractable Eqs. (1)–(2) will be written in front-attached Bertrand intrinsic coordinates, instantaneously normal and parallel to the interface. Details of the transformation between Cartesian and Bertrand coordinates may be found in [13, 14, 15]. For brevity we restrict the discussion to two dimensions. Results of the extension to three dimensions will be outlined in Sec.(8). The Bertrand coordinates (s, n) are related to the Cartesian coordinates $\mathbf{r} = (x, y)$ by the change of variables given by

$$\mathbf{r} = \mathbf{R}(s, t) + n\mathbf{N}(s, t), \tag{6}$$

where $\mathbf{R}(s, t)$ is the position vector of the evolving interface. $\mathbf{N}(s, t)$ is the unit normal to the interface, s is the arclength measured along the interface, and n is the distance from the interface (Figure 2). Note that Bertrand coordinates may produce non-uniqueness similar to that occurring in conventional polar coordinates. This however does not affect the subsequent analysis.

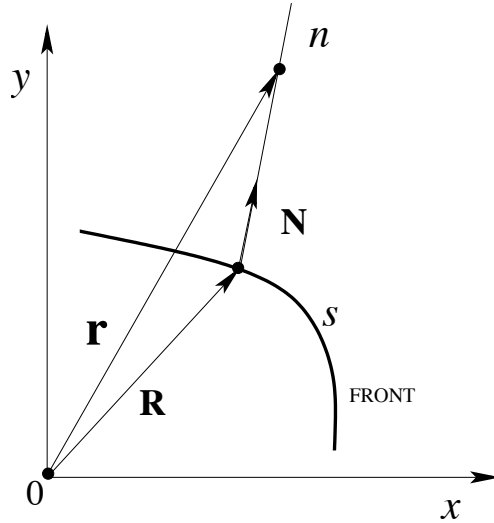


Figure 2: The front-attached orthogonal Bertrand coordinates (n, s) .

In the intrinsic coordinates the flow velocity may be written as,

$$\mathbf{u} = u_s \mathbf{T} + u_n \mathbf{N}, \tag{7}$$

where $\mathbf{T} = \partial \mathbf{R} / \partial s$ is the unit tangent vector to the interface. The diffusion (1) and continuity (2) equations then become,

$$\begin{aligned} \left(\frac{da}{dt} \right)_n - V_n \frac{\partial a}{\partial n} + u_n \frac{\partial a}{\partial n} + \frac{u_s}{1 + n\mathcal{K}} \frac{\partial a}{\partial s} = \\ D \left(\frac{\partial^2 a}{\partial n^2} + \frac{\mathcal{K}}{1 + n\mathcal{K}} \frac{\partial a}{\partial n} + \frac{1}{1 + n\mathcal{K}} \frac{\partial}{\partial s} \left(\frac{1}{1 + n\mathcal{K}} \frac{\partial a}{\partial s} \right) \right), \end{aligned} \tag{8}$$

$$\frac{\partial u_n}{\partial n} + \frac{\mathcal{K}}{1+n\mathcal{K}}u_n + \frac{1}{1+n\mathcal{K}}\frac{\partial u_s}{\partial s} = 0. \quad (9)$$

Here $\mathcal{K}(s, t) = \nabla \cdot \mathbf{N}|_{n=0}$ is the curvature of the interface, $V_n = \partial \mathbf{R} / \partial t \cdot \mathbf{N}$ is its normal velocity. $(da/dt)_n$ is the intrinsic (material) time derivative along the normal. There is a simple relation between the intrinsic time derivative and partial derivative at constant s [13].

$$\left(\frac{da}{dt}\right)_n = \frac{\partial a}{\partial t} + V_s \frac{\partial a}{\partial s}, \quad (10)$$

where $V_s = -\partial \mathbf{R} / \partial t \cdot \mathbf{T}$ is the arclength rate of stretch [13],

$$V_s = \frac{ds}{dt} = \int_0^s \mathcal{K}(\hat{s}, t) V_n(\hat{s}, t) d\hat{s}. \quad (11)$$

For the total arclength L of the evolving interface Eq. (11) yields,

$$\frac{dL}{dt} = \int_0^L \mathcal{K} V_n d\hat{s}. \quad (12)$$

4 Scaling and asymptotic analysis

Assume that at $t = 0$ the interface is weakly curved, that is,

$$\mathcal{K} \sim \varepsilon, \quad \varepsilon \ll 1. \quad (13)$$

ε is an artificial parameter of expansion to provide separation of variables, and which may be interpreted as the diffusive width of the flame times its typical curvature.

Given (13) one may expect that at $t > 0$ the spatio-temporal structure of the solution will involve the short-range variable n , associated with the diffusive layer, and long-range variables $\varepsilon n, \varepsilon s, \varepsilon t$ associated with the curved interface and flow-field away from the interface. Since at $\varepsilon|n| \sim 1$ the concentration is expected to be exponentially close to its limiting values $(0, a_0)$, one may exclude εn from its spatial variables. Thus,

$$a = a(n, \varepsilon s, \varepsilon t). \quad (14)$$

For the stepwise dependency (5) the hydrodynamic field is not directly affected by the processes within the diffusive layer, and one therefore n may exclude from its variables (see also Sec. 8). Thus,

$$\mathbf{u} = \mathbf{u}(\varepsilon n, \varepsilon s, \varepsilon t). \quad (15)$$

The prior removal of certain variables allows to somewhat reduce algebraic manipulations. In terms of the scaled variables,

$$\varkappa = \mathcal{K}/\varepsilon, \quad \xi = \varepsilon s, \quad \eta = \varepsilon n, \quad \tau = \varepsilon t, \quad (16)$$

Eqs. (8) (9), applied to the diffusive layer ($n \sim 1$), yield,

$$\begin{aligned} (\bar{u}_n - V_n) \frac{\partial a}{\partial n} + \varepsilon \left(\frac{\partial a}{\partial \tau} + (\bar{u}_s + V_s) \frac{\partial a}{\partial \xi} \right) - n\varepsilon \left(\varkappa \bar{u}_n + \frac{\partial \bar{u}_s}{\partial \xi} \right) \frac{\partial a}{\partial n} = \\ D \frac{\partial^2 a}{\partial n^2} + \varepsilon \varkappa D \frac{\partial a}{\partial n} + O(\varepsilon^2). \end{aligned} \quad (17)$$

Here,

$$\bar{u}_n = u_n(n=0, \xi, \tau), \quad \bar{u}_s = u_s(n=0, \xi, \tau) \quad (18)$$

are components of the velocity of the flow evaluated at the interface. Equation (17) is considered jointly with conditions,

$$a(n \rightarrow -\infty, \xi, \tau) = a_0, \quad a(n \geq 0, \xi, \tau) = 0,$$

$$\left[\frac{\partial a(n, \xi, \tau)}{\partial n} \right] \Big|_{n=0} = \frac{b_0}{D} \left(\frac{\rho_s}{\rho_g} \right) V_n. \quad (19)$$

Equation (17) is then solved by means of the conventional asymptotic expansion,

$$\begin{aligned} a &= a^{(0)} + \varepsilon a^{(1)} + O(\varepsilon^2), \\ \bar{u}_n &= \bar{u}_n^{(0)} + \varepsilon \bar{u}_n^{(1)} + O(\varepsilon^2), \quad \bar{u}_s = \bar{u}_s^{(0)} + O(\varepsilon), \\ V_n &= V_n^{(0)} + \varepsilon V_n^{(1)} + O(\varepsilon^2), \quad V_s = V_s^{(0)} + O(\varepsilon). \end{aligned} \quad (20)$$

For the leading order asymptotics the problem (17) (19) yields,

$$\begin{aligned} a^{(0)} &= a_0 \left(1 - \exp \left(\frac{\bar{u}_n^{(0)} - V_n^{(0)}}{D} \right) n \right), \quad n < 0 \\ a^{(0)} &= 0, \quad n \geq 0, \end{aligned} \quad (21)$$

with

$$V_n^{(0)} = \frac{a_0}{a_0 + \left(\frac{\rho_s}{\rho_g} \right) b_0} \bar{u}_n^{(0)}. \quad (22)$$

Substituting, (20) into Eq. (17), integrating in the normal direction from $-\infty$ to 0, and taking into account conditions (19), one obtains,

$$\begin{aligned} &\left(a_0 + b_0 \left(\frac{\rho_s}{\rho_g} \right) \right) V_n - a_0 \bar{u}_n + \varepsilon a_0 \kappa D = \\ &-\varepsilon \int_{-\infty}^0 \left(\frac{\partial a^{(0)}}{\partial \tau} + (\bar{u}_s + V_s) \frac{\partial a^{(0)}}{\partial \xi} \right) dn + \varepsilon \int_{-\infty}^0 n \left(\kappa \bar{u}_n + \frac{\partial \bar{u}_s}{\partial \xi} \right) \frac{\partial a^{(0)}}{\partial n} dn + O(\varepsilon^2). \end{aligned} \quad (23)$$

Hence, employing Eqs. (21), (22) and Eq. (11), one obtains,

$$V_n = \frac{a_0}{a_0 + \left(\frac{\rho_s}{\rho_g} \right) b_0} \bar{u}_n + D \left(\frac{\rho_g}{\rho_s} \right) \left(\frac{a_0}{b_0} \right) \left[\frac{\partial}{\partial t} \left(\frac{1}{\bar{u}_n} \right) + \frac{\partial}{\partial s} \left(\frac{\bar{u}_s + V_s}{\bar{u}_n} \right) \right]. \quad (24)$$

Here Eq. (24) is written in the original unscaled variables s, t . Eq. (24) may be further simplified if one recalls that $\rho_s \gg \rho_g$. In this situation scaling t and V_s as (see Eq. (11) and Eq. (44) below),

$$t \sim (\rho_s/\rho_g) \gg 1, \quad V_s \sim (\rho_g/\rho_s) \ll 1, \quad (25)$$

Eq. (24) reduces to,

$$V_n = \left(\frac{\rho_g}{\rho_s} \right) \left(\frac{a_0}{b_0} \right) \left[\bar{u}_n + D \frac{\partial}{\partial s} \left(\frac{\bar{u}_s}{\bar{u}_n} \right) \right]. \quad (26)$$

Eq. (26) effectively replaces the diffusion-advection equation (1) in this asymptotic regime. For a prescribed flow-field \mathbf{u} Eq. (26) defines a second-order differential equation in which the second term on the right ensures dissipation of short-wavelength corrugations, rendering the associated initial-value problem well-posed. The second-order nature of Eq. (26) becomes more transparent if one recalls that $\bar{u}_s = \mathbf{u} \cdot \partial \mathbf{R} / \partial s|_{n=0}$. It is interesting that the dissipation term similar to that of Eq. (26) appears in the early SVF models of premixed gas flames as a part of the total stretch, the combined effect of the interface curvature and the local flow-strain [16],[17]. According to Eq. (26), the interface dynamics is affected by the strain but not by the curvature, as occurs in premixed flames. In terms of the pressure Eq. (26) may be written in the form (see Eqs.(4) and (5)),

$$V_n = \left(\frac{\rho_g}{\rho_s} \right) \left(\frac{a_0}{b_0} \right) \left[\bar{u}_n - D\lambda_b \frac{\partial}{\partial s} \left(\frac{1}{\bar{u}_n} \frac{\partial \bar{P}}{\partial s} \right) \right], \quad (27)$$

advantageous for further analysis. Here, $\bar{P}(s, t) = P(n = 0, s, t)$ is the pressure evaluated at the interface. Recall that due to Eqs. (2) (5),

$$\nabla \cdot (\lambda \nabla P) = 0, \quad (28)$$

implying continuity of the pressure across the interface and, hence, discontinuity of the tangential velocity $\bar{u}_s = \lambda \partial P / \partial s$, provided $\lambda_a \neq \lambda_b$.

5 Evaluation of \bar{u}_n

By virtue of the stepwise dependency (5) the pressure beyond the interface is described by the Laplace equation,

$$\nabla^2 P = 0, \quad (29)$$

which should be considered jointly with the jump conditions on the front,

$$[\nabla P \cdot \mathbf{N}]|_{n=0} = (\lambda_b^{-1} - \lambda_a^{-1})\bar{u}_n, \quad (30)$$

$$[P]|_{n=0} = 0. \quad (31)$$

Equation (30) is a straightforward consequence of Eqs. (4) (5).

A further analysis of the system may therefore be conducted in the framework of the classical theory of logarithmic potential, allowing to connect the shape of the interface with the normal velocity \bar{u}_n and pressure P appearing in Eq. (27). In this paper the discussion is restricted to the most simple situation where the smolder front is a closed curve \mathcal{L} evolving through a two-dimensional flow sustained by a point-source of a prescribed intensity Q (Figure 1),

$$\mathbf{u} = \frac{Q}{2\pi} \frac{\mathbf{r}}{|\mathbf{r}|^2} \quad \text{at } \mathbf{r} \rightarrow 0. \quad (32)$$

The solution of the problem defined by Eqs. (29)-(32) then reads,

$$P(\mathbf{r}, t) = \frac{Q}{2\pi\lambda_b} \ln \frac{1}{|\mathbf{r}|} + \frac{1}{2\pi} \left(\frac{1}{\lambda_a} - \frac{1}{\lambda_b} \right) \int_{\mathcal{L}} \bar{u}_n(\hat{\mathbf{r}}, t) \ln \frac{1}{|\mathbf{r} - \hat{\mathbf{r}}|} d\mathcal{L}_{\hat{\mathbf{r}}}. \quad (33)$$

On the b - side of the front corresponding to $n = -0$ we have,

$$\begin{aligned} \frac{\partial P}{\partial n} \Big|_{n=-0} &= -\frac{Q\mathbf{r} \cdot \mathbf{N}}{2\pi\lambda_b|\mathbf{r}|^2} + \frac{1}{2} \left(\frac{1}{\lambda_a} - \frac{1}{\lambda_b} \right) \bar{u}_n(\mathbf{r}, t) - \\ &\frac{1}{2\pi} \left(\frac{1}{\lambda_a} - \frac{1}{\lambda_b} \right) \int_{\mathcal{L}} \frac{\bar{u}_n(\hat{\mathbf{r}}, t)(\mathbf{r} - \hat{\mathbf{r}}) \cdot \mathbf{N}(\hat{\mathbf{r}}, t)}{|\mathbf{r} - \hat{\mathbf{r}}|^2} d\mathcal{L}_{\hat{\mathbf{r}}}. \end{aligned} \quad (34)$$

The pertinent calculations may be found in [18]. According to Eq. (4),

$$\frac{\partial P}{\partial n} \Big|_{n=-0} = -\frac{1}{\lambda_b} \bar{u}_n. \quad (35)$$

Eqs. (35) and (34) then imply,

$$\begin{aligned} \frac{Q\mathbf{r} \cdot \mathbf{N}}{2\pi\lambda_b|\mathbf{r}|^2} &= \frac{1}{2} \left(\frac{1}{\lambda_a} + \frac{1}{\lambda_b} \right) \bar{u}_n(\mathbf{r}, t) - \\ &\frac{1}{2\pi} \left(\frac{1}{\lambda_a} - \frac{1}{\lambda_b} \right) \int_{\mathcal{L}} \frac{\bar{u}_n(\hat{\mathbf{r}}, t)(\mathbf{r} - \hat{\mathbf{r}}) \cdot \mathbf{N}(\hat{\mathbf{r}}, t)}{|\mathbf{r} - \hat{\mathbf{r}}|^2} d\mathcal{L}_{\hat{\mathbf{r}}}. \end{aligned} \quad (36)$$

Eqs. (27), (33) and (36) fully determine the dynamics of the interface.

6 Numerical strategy

The normal advancement of the interface $\mathbf{R} = (x(s, t), y(s, t))$ at the rate V_n is automatically ensured if one sets,

$$\frac{\partial x}{\partial t} + V_s \frac{\partial x}{\partial s} = V_n \frac{\partial y}{\partial s}, \quad (37)$$

$$\frac{\partial y}{\partial t} + V_s \frac{\partial y}{\partial s} = -V_n \frac{\partial x}{\partial s}, \quad (38)$$

where $0 \leq s \leq L(t)$, and V_s and L are defined by Eqs. (11) (12) with $\mathcal{K} = y_{ss}x_s - x_{ss}y_s$, $x_s^2 + y_s^2 = 1$.

Eqs. (37), (38) are purely geometrical statements valid for any V_n . The front dynamics is specified by the relation (27), where \bar{u}_n is defined by Eq. (36) and P by Eq. (33). Eqs. (37) (38) are considered jointly with the following periodic boundary conditions,

$$x(0, t) = x(L, t), \quad y(0, t) = y(L, t), \quad x_s(0, t) = x_s(L, t), \quad y_s(0, t) = y_s(L, t). \quad (39)$$

The boundary conditions should be supplemented by initial conditions,

$$x(s, 0) = x_0(s), \quad y(s, 0) = y_0(s), \quad L(0) = L_0. \quad (40)$$

The quasi-steady nature of Eq. (36) prevents evaluation of \bar{u}_n as a solution of an initial value problem. Yet, \bar{u}_n can be successfully calculated through the iterative procedure described in [18]. As the zeroth approximation one may take $(\bar{u}_n)_0$ pertaining to the undisturbed radial flow. The initial conditions are conveniently given in terms of the auxiliary angle $0 \leq \theta(s) < 2\pi$,

$$x_0(s) = R(\theta(s)) \cos \theta(s), \quad y_0(s) = R(\theta(s)) \sin \theta(s), \quad (41)$$

where θ and s are related by the equation

$$s(\theta) = \int_0^\theta \sqrt{\left(\frac{dx_0}{d\hat{\theta}}\right)^2 + \left(\frac{dy_0}{d\hat{\theta}}\right)^2} d\hat{\theta}. \quad (42)$$

Hence, $L_0 = s(2\pi)$. The profile $R(\theta)$ is specified as,

$$R(\theta) = R_0 \left[1 + \alpha \left(\cos 5\theta + \frac{1}{3} \sin 13\theta + \frac{1}{10} \cos 27\theta \right) \right]. \quad (43)$$

Note that at $\alpha \ll 1$, $L_0 = 2\pi R_0(1 + O(\alpha^2))$.

7 Numerical simulations

For the forward smoldering sustained by the point source (32) the system does not have an intrinsic length-scale. Hence,

$$r_{ref} = \frac{L_0}{2\pi}, \quad u_{ref} = \frac{Q}{r_{ref}}, \quad t_{ref} = \left(\frac{\rho_s}{\rho_g}\right) \left(\frac{b_0}{a_0}\right) \left(\frac{r_{ref}}{u_{ref}}\right), \quad P_{ref} = \frac{Q}{\lambda_b}, \quad (44)$$

are utilized as the reference length, velocity, time, and pressure-scales, respectively. We also set,

$$\nu = \frac{\lambda_a}{\lambda_b}, \quad \gamma = \frac{D}{Q} \quad (45)$$

which may be regarded as the relative mobility and scaled diffusivity, respectively.

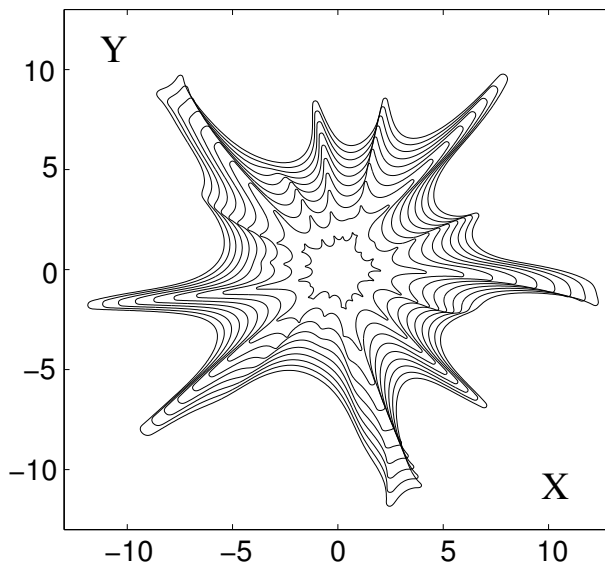


Figure 3: Smoldering front at several consecutive instants of time. $(X, Y) = (x, y)/r_{ref}$. The time interval between the plotted curves is set at $\Delta t = 20t_{ref}$, $4t_{ref} < t < 180t_{ref}$.

Figure 3 presents results of numerical simulations for the initial conditions (43) at $\nu = 0.125$, $\gamma = 0.001$ and $\alpha = 0.1$. Note the cusp-leading nature of the emerging fingering structure. This is

opposite to the cusp-trailing structure occurring in premixed gas cellular/wrinkled flames [16]. With the passage of time, the growth of some small-scale cusps slows down resulting in their absorption by large-scale structures. Simultaneously some well developed cusps swell up and split - quite an unusual behavior in pattern forming systems.

8 Concluding remarks

In modelling fingering instability we tried to bring into the formulation only the most essential ingredients in their simplest form. Since the instability in question is conditioned by the mobility contrast, the simplest way to elucidate its impact is through adoption of the stepwise dependency (5). This is by no means an overly drastic assumption as far as the physical understanding is concerned. In principle, in the limit of strong scale separation considered in the paper, the problem remains perfectly tractable even when the mobility varies in a continuous fashion. In this situation the hydrodynamic field acquires a finite width boundary layer ($n \sim 1$) along the front. The associated mathematical problem may be tackled by the conventional machinery of matched asymptotic expansions. The emergence of the boundary layer, however, cannot affect the large-scale (outer) dynamical picture, which will still be governed by Eq. (27).

Eq. (27) pertains to the 2D-geometry. In the extension over the 3D-case two surface variables are required generating many additional terms in the derivation. The pertinent machinery may be found in [15]. Yet, the heavy algebra notwithstanding, the final relation remains relatively compact. As may be shown, the pressure term $\frac{\partial}{\partial s} \left(\frac{1}{\bar{u}_n} \frac{\partial P}{\partial s} \right)$ of Eq. (27) is merely replaced by $-\mathbf{N} \cdot \text{curl}((\nabla P \times \mathbf{N}) / \bar{u}_n)|_{n=0}$.

The current study deals with the fingering instability sustained by the mobility increase. Yet, the recent study by Aldushin and Matkowsky [10] suggests that a similar kind of instability is likely to be induced also by gasification of the solid reactant. In the present study the gas production is suppressed, and it would be interesting to ascertain its impact on the overall dynamical picture.

To observe fingering in forward smoldering the aspect ratio of the system should be large enough. This apparently may explain the lack of experimental evidence on the phenomenon. We hope that the above findings will stimulate the interest of experimentalists in this problem.

Acknowledgments

The research of IB and GS has been supported by the US-Israel Binational Science Foundation (Grant 2006-151), and the Israel Science Foundation (Grant 350/05). The work of PG was supported in a part by NSF grant DMS-0554775. GS thanks Michael Frankel for helpful discussions.

References

- [1] Ohlemiller, T. J., The SFPE Handbook of Fire Protection Engineering, 3rd ed., 1995, pp. 2.171-2.179.
- [2] Ohlemiller T. J., Prog. Energy Combust. Sci., 65: 277-310 (1986).
- [3] Torero, J. L., and Fernandez-Pello, A.C., Combust. Flame, 106: 89-109 (1996).
- [4] Tse, S. D., Fernandez-Pello, A.C., Miyasaka, K., Twenty-Sixth Symposium (International) on Combustion, the Combustion Institute, 1996, Vol. 1, pp. 1505-1513.
- [5] Dosanjh, S. S., Pagni, P. J., and Fernandez-Pello, A. C., Proceedings of the 1987 ASME/JSME Thermal Engineering Joint Conference, 1987, pp.165-173.

- [6] J. Buckmaster, D. Lozinsky, *Combust. Flame*, 104: 300-310 (1996).
- [7] Schult, D. A., Matkowsky, B. J., Volpert, V.A., and Fernandez-Pello, A. C., *Combust. Flame*, 104: 1-26 (1996).
- [8] Leach, S. V., Rein, G., Ellzey, J. L., and Ezekoye, O. A., *Combust. Flame*, 120: 346-358 (2000).
- [9] Aldushin, A. P., *Combust. Flame*, 94: 308-320 (1993).
- [10] Aldushin, A. P., and Matkowsky, B. J., *Combust. Sci. Technol.*, 13: 293-341 (1998).
- [11] Akkutlu, I. Y., and Yortsos, Y. C., *Combust. Flame*, 133: 229-247 (2003).
- [12] Lu, C., and Yortsos, Y. C., *AIChE Journal*, 51: 1279-1296 (2005).
- [13] M. E. Gurtin, *Thermomechanics of Evolving Phase Boundaries on the Plane*. Oxford Univ. Press, 1993.
- [14] J. Yao, S. Stewart, *J. Fluid Mech.*, 309: 225-275 (1996).
- [15] Matalon, M., Cui, C., and Bechtold, J. K., *J. Fluid Mech.*, 487: 179-210 (2003).
- [16] G. I. Sivashinsky, *Acta Astronaut.*, 3: 889-918 (1976).
- [17] M. Matalon, *Combust. Sci. Technol.*, 31: 169-181 (1983).
- [18] I. Brailovsky, A. Babchin, M. Frankel, G. Sivashinsky, *Transp. Porous Media*, 63: 363-380 (2006).
- [19] G. I. Sivashinsky, *Ann. Rev. Fluid Mech.*, 15: 179-199 (1983).